Line Shapes in a Magnetic Field: Trajectory Modifictions II: Full Collision-Time Statistics

Spiros Alexiou

Hellenic Army Academy, Varis—Koropiou Avenue Vari, P.O. 16673 Vari, Greece; moka1@otenet.gr

Abstract: In a previous paper, a variation of the Collision-time Statistics method was applied to identify the relevant perturbers for line broadening under the action of a constant magnetic field. As discussed, that version was simplified and inadequate for low magnetic field and/or large perturber mass (ions). The purpose of the present work is to augment the previous work, so that such cases can be handed efficiently. The results may also be used to construct analytic, i.e., impact/unified models under the usual assumptions in these models.

---

1. Introduction

In a previous paper [1], a variation of the Collision-time Statistics method was applied to identify the relevant perturbers for line broadening under the action of a constant magnetic field. As discussed, that version was simplified and inefficient for low magnetic field and/or or large perturber mass (ions), because an unnecessarily large number of perturbers, the vast majority of which only contribute negligibly to broadening, were generated. The purpose of the present work is to augment the previous work, so that such cases can be handled efficiently. The main problem with the previous treatment was the case of large Larmor radii and corresponding slow cyclotron frequencies, as in the case of large perturber mass and/or low magnetic field. In such cases the motion of the perturbers in the plane perpendicular to the magnetic field may be quite far from completing a full cycle. As a result in the simplified treatment of [1] a large number of ineffective perturbers would be included in that case. It is believed [2] that "as long as the gyro-radii of the electrons are much larger than the Debye sphere" the particle trajectories, or, equivalently, the dielectric function would be unaffected by the magnetic field, since the perpendicular motion involves presumably much smaller length scales than the parallel motion, although this belief remains to be quantified. It is shown here that this criterion is not quite correct and that the key parameter determining the adequacy of neglecting spiralling is the ratio of the cyclotron frequency to the width of the line in question.

2. Theoretical Formulation

As in [1] we assume that:

a.   the distribution functions, e.g., the Maxwellian velocity distribution is *not* affected by the B-field.
b.   the shielding is also not affected, e.g., Debye screening

We also consider a neutral emitter in this work.

2.1. Collision-Time Statistics

To include *all* and only the relevant perturbers, we use a modification of the collision-time statistics method of Hegerfeld and Kesting [3] with Seidel's improvement [4]- see Ref. [5] for details, as discussed in [1].

As in [1], perturbers move in a helical path characterized by the parallel constant velocity v_z, where the magnetic field direction defines the z-axis (passing through the emitter), the perpendicular velocity with magnitude $v_\perp$ and impact parameter ρ, which is the distance of the center of the spiral to the z-axis, i.e., the perpendicular motion in the x-y plane is a circular motion with the Larmor radius $r_L = \frac{v_\perp}{\omega_L}$ around the center ρ, with $\omega_L = |Q|B/m$ the cyclotron frequency and Q the perturber charge. For the impact parameter ρ

$$max(0, r_L - R_{max}) \leq \rho \leq R_{max} + r_L, \tag{1}$$

i.e., the impact parameter lies in a disk or annulus depending on whether the range R_{max} of the interaction, discussed below, is larger or smaller than r_L.

The relevant quantities for the helical trajectory **R**(t) are as follows: The z-coordinate of the trajectory is

$$R_z(t) = v_z(t - t_i) = v_z t + z_0, \tag{2}$$

with

$$z_0 = -v_z t_i, \tag{3}$$

with the times of closest approach t_i representing the time the perturber trajectory intersects the x-y plane and being uniformly distributed. z_0 thus represents how far from the x-y plane the perturber is at $t = 0$.

Hence

$$R_x(t) = \rho \cos\theta + r_L \cos(\omega_L t + \psi), R_y(t) = \rho \sin\theta + r_L \sin(\omega_L t + \psi) \tag{4}$$

where θ describes the position of the impact parameter vector in the x-y plane and is uniformly distributed in $(0, 2\pi)$. ψ is an angle describing where on the circular trajectory projection the perturber finds itself at $t = 0$ and is also uniformly distributed in $(0, 2\pi)$ and ultimately related to the time the B-field was turned on. Each perturber is thus characterized by the vector $(v_z, v_\perp, \rho, \theta, \psi, t_i)$, or equivalently z_0 instead of t_i.

As in [1] we consider as "relevant " perturbers those that, at any time during the interval of interest $(0, \tau)$, come closer to the emitter than a distance R_{max}, defined so that the interaction is negligible for distances larger than R_{max}. For a Debye interaction, we usually take $R_{max} \approx 3\lambda_D$, where λ_D denotes the shielding(Debye) length. This is because the interation becomes negligible ($\leq 3\%$ for larger distances).

Therefore for a perturber to be relevant the condition $R(t) \leq R_{max}$ must hold for at least one time t in $(0, \tau)$, where τ is the time of interest, i.e., a time large enough that the Fourier transform of the line profile $C(t)$ has decayed to negligible levels, or an asymptotic form is identifiable. $C(t)$ is a linear combination of products of time evolution operators (U-matrices) of the upper and lower levels. These time evolution operators -needed for times $0 \leq t \leq \tau$- are determined by solving the Schroedinger equation in the Debye-shielded field $V(t)$. Therefore a particle will only be relevant if for at least one time in the interval $[0, \tau]$ it comes closer than R_{max} to the emitter(if not, then the perturbation produced by that particle is negligible due to Debye screening), which means that for at least *one* time t in $[0, \tau]$:

$$(v_z t + z_0)^2 + (\rho \cos\theta + r_L \cos(\omega_L t + \psi))^2 + (\rho \sin\theta + r_L \sin(\omega_L t + \psi))^2 \leq R_{max}^2 \tag{5}$$

This reads:

$$R_{max}^2 - (v_z t - v_z t_i)^2 \geq \rho^2 + r_L^2 + 2\rho r_L \cos(\omega_L t + \psi - \theta) \tag{6}$$

Thus we generate $v_z, v_\perp, \rho, t_i$ and θ as before, but also draw ψ, uniformly distributed in $(0, 2\pi)$ as illustrated in in Figure 1 and effectively only accept perturbers if, for at least one time in $(0, \tau)$ Equation (6) is satisfied. The *maximum* value of the LHS occurs for $t = t_i$. This in general imposes *restrictions* (i.e., not all ψ contribute for a given θ) on the values of θ and ψ that a perturber can have and still contribute effectively to broadening, specifically:

a.   If $r_L < R_{max}$ and $\rho \leq R_{max} - r_L$, $R_{max} \geq \rho + r_L$ and Equation (6) is satisfied for $t = t_i$ for *any* θ, ψ and $\omega_L t$. Therefore in this case we have no restriction and θ and ψ can independently take any value.

b.   In all other cases, Equation (6) results in the restriction:

$$\arccos\left(\frac{R_{max}^2 - \rho^2 - r_L^2}{2\rho r_L}\right) \leq |\omega_L t + \psi - \theta| \tag{7}$$

Note that for Case b, the argument of the inverse cosine is absolutely ≤ 1. Specifically:

1.   If $r_L \geq R_{max}$, then

$$0 \geq \frac{R_{max}^2 - r_L^2 - \rho^2}{2\rho r_L} \geq -1 \tag{8}$$

The left of the inequality follows because $R_{max} \leq r_L$ alone. The right part also follows since

$$r_L - R_{max} \leq \rho \leq r_L + R_{max} \Rightarrow -R_{max} \leq \rho - r_L \leq R_{max} \tag{9}$$

Hence

$$R_{max}^2 \geq \rho^2 + r_L^2 - 2\rho r_L \Rightarrow \frac{R_{max}^2 - r_L^2 - \rho^2}{2\rho r_L} \geq -1 \tag{10}$$

2.   For $r_L \leq R_{max}$, Equation (9) is also valid since $r_L - R_{max} \leq 0 \leq \rho$, as is Equation (10). Since, as already discussed the case $\rho \leq R_{max} - r_L$ imposes no restriction, we only consider here the case $R_{max} - r_L \leq \rho \leq R_{max} + r_L$, which implies $\rho - r_L \leq R_{max} \leq \rho + r_L$. It thus remains to show that

$$\frac{R_{max}^2 - r_L^2 - \rho^2}{2\rho r_L} \leq 1 \tag{11}$$

which follows from $R_{max} \leq \rho + r_L$.

Thus

a.   For $r_L \leq R_{max}, \rho \leq r_L$, Equation (6) is satisfied for $t = t_i$ for any θ, ψ and $\omega_L t$ and there is no restriction on ψ, θ and $\omega_L t$.

b.   In all other cases, the restriction imposed by Equation (7) applies and the argument of the inverse cosine is always absolutely ≤ 1.

Hence the angle difference $\psi - \theta$ must be in the shaded area shown in Figure 2. So for at least one time t in $(0, \tau)$, the following must hold for the perturber with parameters ρ, r_L, θ, ψ to contribute:

$$|\psi + \omega_L t - \theta| \geq \arccos\left(\frac{R_{max}^2 - \rho^2 - r_L^2}{2\rho r_L}\right). \tag{12}$$

i.e.,

$$\psi + \omega_L t \geq \theta + \arccos\left(\frac{R_{max}^2 - \rho^2 - r_L^2}{2\rho r_L}\right), \psi + \omega_L t \geq \theta \tag{13}$$

or

$$\theta - \arccos\left(\frac{R_{max}^2 - \rho^2 - r_L^2}{2\rho r_L}\right) \geq \psi + \omega_L t, \theta \geq \psi + \omega_L t \tag{14}$$

The net result is that for each θ, only a a range of ψ,

$$\Delta\psi \leq 2\left(\pi - \arccos\left(\frac{R_{max}^2 - \rho^2 - r_L^2}{2\rho r_L}\right)\right) + \omega_L \tau \tag{15}$$

contributes (this means that a fraction $\frac{\Delta\psi}{2\pi}$ contributes compared to the simplified case discussed in the previous work, i.e., the collision volume is smaller by $\frac{\Delta\psi}{2\pi}$). If this is $\ll 1$ we effectively have rectilinear

trajectories for the time of interest. If this turns out to be larger than 2π, we have a full revolution and we can use the simplified formulas discussed in [1]. As mentioned, we are mainly interested in the situation where $R_{max} < r_L$ and $\omega_L \tau < 2\pi$, as this is the case of large r_L, but slow ω_L, otherwise the relation between ψ and θ is always satisfied for at least one t in $(0, \tau)$.
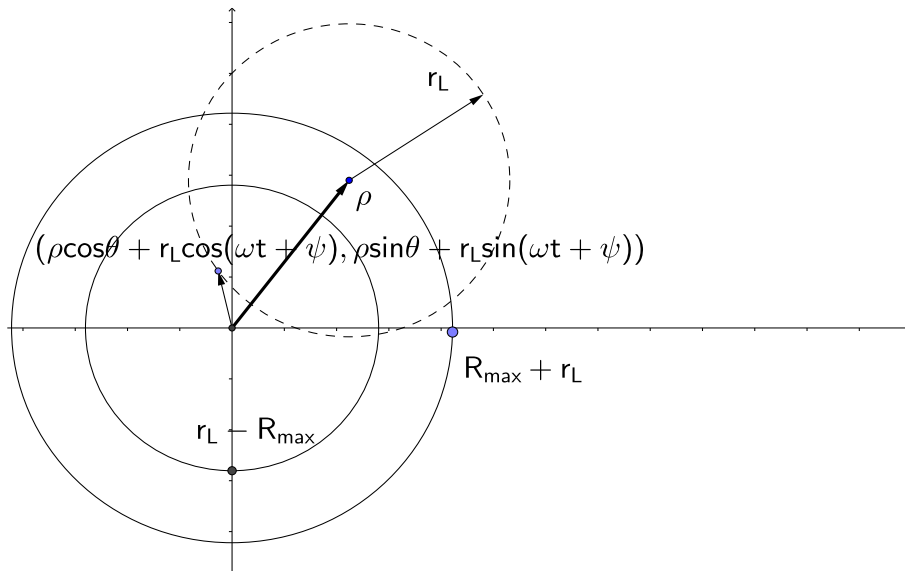
Figure 1. x-y trajectory projections for $r_L \geq R_{max}$. Shown is the annular region between concentric circles with the origin (the emitter position) as center and radii $r_L - R_{max}$ and $r_L + R_{max}$, respectively. For an impact parameter at a distance ρ from the center in the annular region, a circle with radius r_L (dashed) represents the projection of the perturber path in the x-y plane. Hence a point on that circle is $\left(\rho \cos\theta + r_L \cos(\omega t + \psi), \rho \sin\theta + r_L \sin(\omega t + \psi)\right)$, with ψ the angle on the dashed circle. This must be no more than R_{max} away from the center, else this perturber does not contribute.
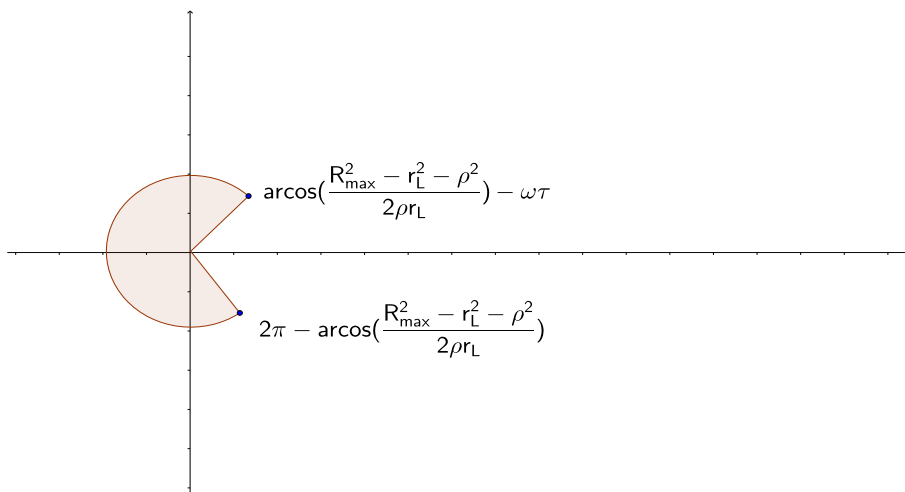
Figure 2. The shaded area shows the difference $\psi - \theta$ that satisfies Equation (6).

We can use the variable $x = \rho - r_L$ with $-R_{max} \leq x \leq R_{max}$ and write the argument of the inverse cosine as

$$\frac{R_{max}^2 - \rho^2 - r_L^2}{2\rho r_L} = \frac{R_{max}^2 - x^2}{2r_L(x + r_L)} - 1 \tag{16}$$

Note that for low B (large r_L) this tends to -1, hence the inverse cosine is close to π. This means that in this limit $|\psi - \theta| \approx \pi$, e.g., we get a $\Delta\psi \approx 0$ (but note that in that limit we had divergencies in the relevant functions when computing the collision volume in [1]).

This situation is depicted in Figure 3, which shows the typical situation for the phase space of the quantity $\psi - \theta$ that contributes. This is also illustrated in Figure 4, which shows, for the same ρ, 4 different angles θ, which determine the centers of the spirals and the parts of the circular projections of these spirals that are effective. For instance if the center of the spiral, i.e., the vector of the impact parameter is the the right ($\theta \approx 0$), then $\psi \approx \pi$ (the leftmost of the circular trajectory projection) for $r_L \gg R_{max}$. Similarly, if the impact parameter vector is to the south ($\theta \approx 3\pi/2$), then the relevant ψ is to the north of the circular trajectory projection, e.g., $\psi \approx \pi/2$).
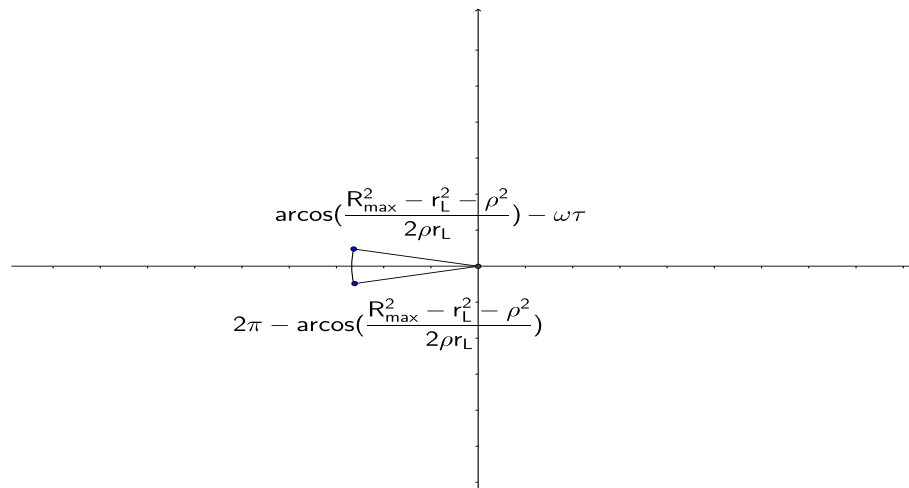

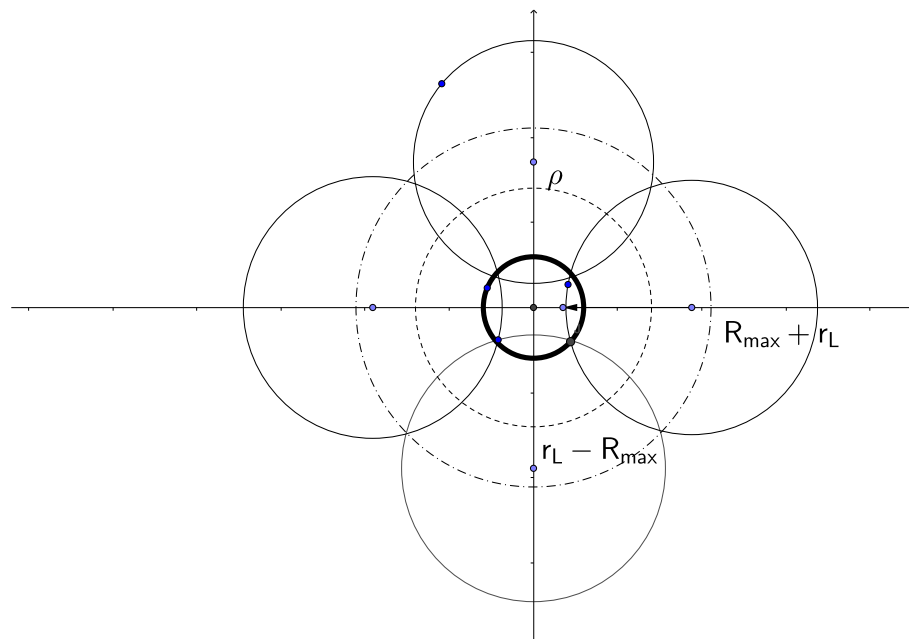**Figure 3.** The shaded area shows the difference $\psi - \theta$ that satisfies Equation (6).

Figure 4. Illustration of the relation between θ and ψ for the case $r_L \gg R_{max}$. Impact parameters ρ lie between the dashed and dash-dotted circles with radii $r_L - R_{max}$ and $r_L + R_{max}$. The part of the circular trajectory projections that are within R_{max} (bold circle) of the emitter (i.e., the center) are in the opposite direction of the impact parameter vector, e.g., to the north for the southern circular trajectory projection.

In the limit $B = 0$ (or infinite perturber mass), $\arccos(\frac{R_{max}^2 - \rho^2 - r_L^2}{2\rho r_L}) = \pi$ and we get from the θ and ψ integrations a term $\frac{\omega_L \tau}{2\pi}$.

2.2. Collision Volume

The collision-time statistics method first computes the number of relevant particles, i.e., the density times the relevant volume, i.e., the above cylinder. This volume is as before [1], except that we also account for the polar angle θ, describing the orientation of the impact parameter with respect to the x-axis and the angle ψ describing the position of the particle on the perpendicular x-y plane at time $t = 0$, i.e., we have the extra integrations $\int_0^{2\pi} \frac{d\theta}{2\pi} \int_0^{2\pi} \frac{d\psi}{2\pi}$. The ψ integration simply returns a factor of 1 if $\omega_L \tau \geq 2\pi$, but it does so even under the weaker condition $\omega_L \tau \geq 2 \arccos(\frac{R_{max}^2 - \rho^2 - r_L^2}{2\rho r_L})$, or

$$\frac{R_{max}^2 - \rho^2 - r_L^2}{2\rho r_L} \geq \cos(\omega_L \tau / 2) \tag{17}$$

Otherwise it gives a factor of $\frac{\Delta \psi}{2\pi}$ with $\Delta \psi$ defined in Equation (15).
The nonnegative root of Equation (17) is

$$\rho_1 = -\cos(\omega_L \tau / 2) r_L + \sqrt{R_{max}^2 - \sin^2(\omega_L \tau / 2) r_L^2}, \tag{18}$$

i.e., the results of [1] are also valid for $\rho \leq \rho_1$, which in turn requires that

$$R_{max} > r_L \tag{19}$$

(else $\rho_1 \leq 0$) , which also guarantees the reality of ρ_1, i.e.,

$$R_{max} \geq \sin(\omega_L \tau / 2) r_L \tag{20}$$

The θ angular integration simply returns 1 in either case. As a result, the results of [1] need *no modification* for $\omega_L \tau \geq 2\pi$. Otherwise, the collision volume calculation runs as follows:
For $v_\perp < R_{max} \omega_L$, i.e., $r_L < R_{max}$, $\Delta \psi(\rho) = 1$. However, as already discussed, this is valid (e.g., no restriction on ψ is required) also for $\rho < r_L$, hence $\Delta \psi(\rho) = 1$ for $\rho \leq max(r_L, \rho_1) = \rho_2$.
For small R_{max} / r_L and $\omega_L \tau$, r_L is the maximum of the two. The collision volume reads:

$$V = 2\pi \int_{-\infty}^{\infty} f(v_z) dv_z \int_0^{\infty} f_2(v_\perp) dv_\perp \int_{max(0, \frac{v_\perp}{\omega_L} - R_{max})}^{R_{max} + \frac{v_\perp}{\omega_L}} \rho d\rho \Delta \psi(\rho) \int_{-\frac{\sqrt{R_{max}^2 - (\rho - r_L)^2}}{|v_z|}}^{\tau + \frac{\sqrt{R_{max}^2 - (\rho - r_L)^2}}{|v_z|}} dt_i \tag{21}$$

$$= 2\pi \int_{-\infty}^{\infty} f(v_z) dv_z \int_0^{\infty} f_2(v_\perp) dv_\perp \int_{max(0, \frac{v_\perp}{\omega_L} - R_{max})}^{R_{max} + \frac{v_\perp}{\omega_L}} (|v_z| \tau + 2\sqrt{R_{max}^2 - (\rho - r_L)^2}) \Delta \psi(\rho) \rho d\rho$$

$$= 2\pi (C_1 + C_2)$$

with $f(v_z) = \sqrt{\frac{m}{2\pi kT}} e^{-mv_z^2 / 2kT}$ and $f_2(v_\perp) = \frac{m}{kT} v_\perp e^{-mv_\perp^2 / 2kT}$ denoting a one and two-dimensional Maxwellian velocity distributions respectively and with $\Delta \psi$ redefined as in Table 1:

Table 1. $\frac{\Delta \psi(\rho)}{2\pi}$ vs. relevant parameters.

$\omega_L \tau$	$\frac{r_L}{R_{max}}$	$\frac{\rho}{max(\rho_1, r_L)}$	$\frac{\Delta \psi(\rho)}{2\pi}$
$\geq 2\pi$			1
$< 2\pi$	≤ 1	≤ 1	1
$< 2\pi$	≤ 1	> 1	$\left(1 - \frac{\arccos(\frac{R_{max}^2 - \rho^2 - r_L^2}{2\rho r_L})}{\pi}\right) + \frac{\omega_L \tau}{2\pi}$
$< 2\pi$	> 1		$\left(1 - \frac{\arccos(\frac{R_{max}^2 - \rho^2 - r_L^2}{2\rho r_L})}{\pi}\right) + \frac{\omega_L \tau}{2\pi}$

C_1 and C_2 are:

$$
\begin{aligned}
C_1 &= \tau \int_{-\infty}^{\infty} f(v_z)|v_z|dv_z \int_0^{\infty} f_2(v_\perp)dv_\perp \int_{max(0,\frac{v_\perp}{\omega_L}-R_{max})}^{R_{max}+\frac{v_\perp}{\omega_L}} \rho d\rho \Delta\psi(\rho) \\
&= \langle |v_z| \rangle \tau \int_0^{\infty} f_2(v_\perp)dv_\perp \int_{max(0,\frac{v_\perp}{\omega_L}-R_{max})}^{R_{max}+\frac{v_\perp}{\omega_L}} \rho d\rho \Delta\psi(\rho) \\
&= \langle |v_z| \rangle \tau [\int_0^{R_{max}\omega_L} f_2(v_\perp)dv_\perp \int_0^{R_{max}+\frac{v_\perp}{\omega_L}} \rho d\rho \Delta\psi(\rho) + \int_{R_{max}\omega_L}^{\infty} f_2(v_\perp)dv_\perp \int_{\frac{v_\perp}{\omega_L}-R_{max}}^{R_{max}+\frac{v_\perp}{\omega_L}} \rho d\rho \Delta\psi(\rho)] \\
&= \langle |v_z| \rangle \tau R_{max}^2 (I_1 + I_2 + I_3)
\end{aligned}
\tag{22}
$$

with $\langle |v_z| \rangle = \int_{-\infty}^{\infty} |v|f(v)dv = \sqrt{\frac{2kT}{\pi m}}$ The integrals $I_1 - I_3$ are given explicitly below. However, we first define the dimensionless quantities:

$$
s = \frac{v_\perp}{\omega_L R_{max}}
\tag{23}
$$

and

$$
r = \frac{\rho_2}{R_{max}} = max(-\cos(\omega_L\tau/2)s + \sqrt{1-\sin^2(\omega_L\tau/2)s^2}, s)
\tag{24}
$$

and

$$
q = R_{max}\omega_L \sqrt{\frac{m}{2kT}}
\tag{25}
$$

(essentialy the averaged inverse s R_{max}/r_L).

$$
I_1 = R_{max}^{-2} \int_0^{R_{max}\omega_L} f_2(v_\perp)dv_\perp \int_0^{\rho_2} \rho d\rho = \int_0^{R_{max}\omega_L} f_2(v_\perp)dv_\perp \frac{\rho_2^2(v_\perp)}{2}
\tag{26}
$$

$$
I_2 = R_{max}^{-2} \int_0^{R_{max}\omega_L} f_2(v_\perp)dv_\perp \int_{\rho_2}^{R_{max}+\frac{v_\perp}{\omega_L}} \rho((1 - \frac{\arccos(\frac{R_{max}^2-\rho^2-r_L^2}{2\rho r_L})}{\pi}) + \frac{\omega_L\tau}{2\pi})d\rho
\tag{27}
$$

and

$$
I_3 = R_{max}^{-2} \int_{R_{max}\omega_L}^{\infty} f_2(v_\perp)dv_\perp \int_{\frac{v_\perp}{\omega_L}-R_{max}}^{R_{max}+\frac{v_\perp}{\omega_L}} \rho((1 - \frac{\arccos(\frac{R_{max}^2-\rho^2-r_L^2}{2\rho r_L})}{\pi}) + \frac{\omega_L\tau}{2\pi})d\rho
\tag{28}
$$

while

$$
\begin{aligned}
C_2 &= 2\int_{-\infty}^{\infty} f(v_z)dv_z \int_0^{\infty} f_2(v_\perp)dv_\perp \int_{max(0,\frac{v_\perp}{\omega_L}-R_{max})}^{R_{max}+\frac{v_\perp}{\omega_L}} \sqrt{R_{max}^2 - (\rho - r_L)^2}\rho d\rho \Delta\psi(\rho) \\
&= 2\int_0^{\infty} f_2(v_\perp)dv_\perp \int_{max(0,\frac{v_\perp}{\omega_L}-R_{max})}^{R_{max}+\frac{v_\perp}{\omega_L}} \sqrt{R_{max}^2 - (\rho - r_L)^2}\rho d\rho \Delta\psi(\rho) \\
&= 2[\int_0^{R_{max}\omega_L} f_2(v_\perp)dv_\perp \int_0^{R_{max}+\frac{v_\perp}{\omega_L}} \sqrt{R_{max}^2 - (\rho - r_L)^2}\rho d\rho \Delta\psi(\rho) \\
&+ \int_{R_{max}\omega_L}^{\infty} f_2(v_\perp)dv_\perp \int_{\frac{v_\perp}{\omega_L}-R_{max}}^{R_{max}+\frac{v_\perp}{\omega_L}} \sqrt{R_{max}^2 - (\rho - r_L)^2}\rho d\rho \Delta\psi(\rho)] \\
&= 2R_{max}^3 (J_1 + J_2 + J_3)
\end{aligned}
\tag{29}
$$

with

$$
\begin{aligned}
J_1 &= R_{max}^{-3} \int_0^{R_{max}\omega_L} f_2(v_\perp)dv_\perp \int_0^{\rho_2} \sqrt{R_{max}^2 - (\rho - r_L)^2}\rho d\rho \\
&= \int_0^{q^2} dx e^{-x}[\frac{s}{2}(\arcsin(s) - \arcsin(s-r)) + \frac{(s^2+2)\sqrt{1-s^2}-(s^2+2+sr-2r^2)\sqrt{1-s^2+2sr-r^2}}{6}]
\end{aligned}
\tag{30}
$$

with $x = \frac{mv_\perp^2}{2kT}$ and $s = \frac{x^{1/2}}{q}$, r being of course functions of x.

$$
J_2 = R_{max}^{-3} \int_0^{R_{max}\omega_L} f_2(v_\perp)dv_\perp \int_{\rho_2}^{R_{max}+\frac{v_\perp}{\omega_L}} \sqrt{R_{max}^2 - (\rho - r_L)^2}\rho(1 - \frac{\arccos(\frac{R_{max}^2-\rho^2-r_L^2}{2\rho r_L})}{\pi}) + \frac{\omega_L\tau}{2\pi})d\rho
\tag{31}
$$

and

$$J_3 = R_{max}^{-3} \int_{R_{max}\omega_L}^{\infty} f_2(v_\perp) dv_\perp \int_{\frac{v_\perp}{\omega_L} - R_{max}}^{R_{max} + \frac{v_\perp}{\omega_L}} \sqrt{R_{max}^2 - (\rho - r_L)^2} \rho \left(1 - \frac{\arccos(\frac{R_{max}^2 - \rho^2 - r_L^2}{2\rho r_L})}{\pi}\right) + \frac{\omega_L \tau}{2\pi}) d\rho \qquad (32)$$

Note that the *only* difference from the previous work [1] is the factor $\Delta\psi(\rho)$ for $\omega_L \tau < 2\pi$. Also note that in [1], the corresponding integrations to infinity, e.g., the equivalents of I_3 and J_3 diverged as $q \to 0$. This divergence has been eliminated here due to the $\Delta\psi$ factor. This is shown in Appendix A, which evaluates the I_3 and J_3 integrals.

The remaining contributions vanished in [1] as $q \to 0$ and clearly continue to do so here.

As already mentioned in [1], the number of particles that are in this volume, and hence need to be simulated, is simply the volume multiplied by the perturber density.

2.3. Generating Perturbers

To generate perturbers we proceed as in [1], but also generate for each perturber an angle θ, uniformly distributed in (0,2π). Once we have generated $v_z, v_\perp, \rho, t_i$ and θ, we also generate ψ uniformly distributed in $\left(\theta + \arccos(\frac{R_{max}^2 - r_L^2 - \rho^2}{2\rho r_L}) - \omega_L \tau, \theta + 2\pi - \arccos(\frac{R_{max}^2 - r_L^2 - \rho^2}{2\rho r_L})\right)$.

In more detail, we first draw a random number uniformly distributed in (0,1). If this is smaller than $\frac{C_1}{C_1 + C_2}$, then we generate $|v_z|, v_\perp, \rho$ from the distribution $P_1(|v_z|, v_\perp, \rho) = |v_z| f(v_z) f_2(v_\perp) \rho$ by generating independently a v_z with the probability distribution $|v_z| f(v_z)$, a $v_\perp$ with the probability distribution $f_2(v_\perp)$ and a ρ with the probability density $\rho d\rho$ in $\left((max(0, \frac{v_\perp}{\omega_L} - R_{max}), R_{max} + \frac{v_\perp}{\omega_L})\right)$.

Otherwise we generate from the distribution $P_2(|v_z|, v_\perp, \rho) = f(v_z) f_2(v_\perp) \rho \sqrt{R_{max}^2 - (\rho - r_L)^2}$. The generation of impact parameters was done by a rejection method, as straightforward inversion is not possible.

Once $v_z, v_\perp$ and ρ have been generated, t_i is selected as a uniformly distributed time in $(-\sqrt{R_{max}^2 - (\rho - r_L)^2}, |v_z|\tau + \sqrt{R_{max}^2 - (\rho - r_L)^2})$. θ and ψ are also generated as discussed above.

3. Conclusions

The present work extends the simplified theory for spiralling motion in a constant magnetic field presented in [1] which was typically efficient for electron perturbers to more cases of practical interest, i.e., ion perturbers and/or weak magnetic fields. The results of [1] are seen to hold for $\omega_L \tau \geq 2\pi$ and are here extended to $\omega_L \tau < 2\pi$, i.e., a regime typical for ions or weak magnetic field, thus validating the common wisdom that ion trajectories are usually unaffected by spiralling. In addition, this work identifies relevant parameters (e.g., q, $\omega_L \tau$) and criteria for using a straight line and also allows the efficient treatment of spiraling ion trajectories if needed. The results of this work are also a useful basis for approximate standard treatments, i.e., impact/unified theories, if (strong) collisions are isolated/disentangled and further, to perturbative impact/unified treatments if these collisions may be handled in perturbation theory.

With regard to the notion [2], discussed in the introduction, that the relevant quantity for neglecting spiralling is that $r_L \gg R_{max}$, the present paper shows that although the idea is qualitatively correct, i.e., one may indeed neglect spiralling for small B and/or large perturber mass, leading to a large Larmor radius, the actual situation is more complex and described by Table 1. Specifically, to neglect spiralling, it is necessary that $\frac{\omega_L \tau}{2\pi} \ll 1$ or equivalently $\frac{\omega_L}{HWHM} \ll 1$, i.e., the ratio of the cyclotron frequency to the width(HWHM) of the line is important. This is because if this ratio is small, then the perturber motion does not cover a full revolution and if very small, the motion is essentially unaffected by the magnetic field. However, if the line is very narrow (τ is large) there may be enough time to complete at least a sizeable portion of a revolution, even if the Larmor radius is larger than the Debye length.

Conflicts of Interest: The author declares no conflict of interest.

Appendix A. Calculation of the I_3 and J_3 Double Integrals

Note that the integrands are the same except that J_n involves and extra factor of $\sqrt{R_{max}^2 - (\rho - r_L)^2}$.

Note that these integrals are the *only* contributions for $q = 0$ ($B = 0$).

Appendix A.1. The I_3 Integration

For I_2 and I_3, the non-trivial ρ integrals reduce to ($x = \rho/R_{max}$)

$$\int dx\, x \arccos\left(\frac{1-x^2-s^2}{2xs}\right) = \frac{1}{4}\left[2x^2\arccos\left(\frac{1-x^2-s^2}{2xs}\right) + \sqrt{-s^4 + 2s^2(x^2+1) - (x^2-1)^2}\right] + \frac{1}{2}\arctan\left(\frac{1+s^2-x^2}{\sqrt{-s^4+2s^2(x^2+1)-(x^2-1)^2}}\right) \tag{A1}$$

For both I_2 and I_3, the upper limit if $s + 1$, for which

$$\arccos\left(\frac{1-x^2-s^2}{2xs}\right) = \arccos(-1) = \pi \tag{A2}$$

and

$$\sqrt{-s^4 + 2s^2(x^2+1) - (x^2-1)^2} = 0 \tag{A3}$$

Hence the middle term vanishes, while the arctangent is

$$\arctan\left(\frac{1+s^2-x^2}{\sqrt{-s^4+2s^2(x^2+1)-(x^2-1)^2}}\right) = \arctan\left(\frac{-2s}{0^+}\right) = -\frac{\pi}{2} \tag{A4}$$

If (as in I_3) the lower limit is $s - 1$, the argument of the square root is also 0, $\arccos\left(\frac{1-x^2-s^2}{2xs}\right) = \arccos(-1) = \pi$ and

$$\arctan\left(\frac{1+s^2-x^2}{\sqrt{-s^4+2s^2(x^2+1)-(x^2-1)^2}}\right) = \arctan\left(\frac{2s}{0^+}\right) = \frac{\pi}{2} \tag{A5}$$

I_3 is

$$\begin{aligned}
I_3 &= \int_{R_{max}\omega_L}^{\infty} dv_\perp f_2(v_\perp) \int_{s-1}^{s+1} dx\, x\left(1 + \frac{\omega_L\tau}{2\pi} - \frac{\arccos\frac{1-x^2-s^2}{2xs}}{\pi}\right) \\
&= \int_{R_{max}\omega_L}^{\infty} dv_\perp f_2(v_\perp)\left(2s(1 + \frac{\omega_L\tau}{2\pi}) - \frac{4s-1}{2}\right) = \left[\frac{e^{-q^2}}{2} + \frac{\omega_L\tau}{2\pi}\frac{2}{q}\int_{q^2}^{\infty} dx\, x^{1/2}e^{-x}\right] \\
&= \left[\frac{e^{-q^2}}{2} + \frac{2\omega_L\tau}{2\pi}\left(e^{-q^2} + \pi^{1/2}\frac{1-erf(q)}{2q}\right)\right] = \frac{e^{-q^2}}{2}\left(1 + \frac{2\omega_L\tau}{\pi}\right) + (1 - erf(q))\frac{\langle|v_z|\rangle\tau}{2R_{max}}
\end{aligned} \tag{A6}$$

Note that unlike the simplified version [1], I_3 does *not* diverge because the $\omega_L\tau$ cancells the q^{-1}.

The J_3 Integration

We break the J_3 integral as

$$J_3 = J_{31} + J_{32} \tag{A7}$$

where using $s = \frac{v_\perp}{R_{max}\omega_L}$, we have:

$$\begin{aligned}
J_{31} &= \frac{\omega_L\tau}{2\pi}\int_{R_{max}\omega_L}^{\infty} dv_\perp f_2(v_\perp)\int_{s-1}^{s+1} dx\, x\sqrt{1-(x-s)^2} = 2q^2\frac{\omega_L\tau}{2\pi}\int_1^{\infty} se^{-s^2q^2}\frac{s\pi}{2} \\
&= \frac{\pi}{2}\frac{\omega_L\tau}{2\pi}\left[\sqrt{\pi}\frac{1-erf(q)}{2q} + e^{-q^2}\right] = \frac{\omega_L\tau e^{-q^2}}{4} + \frac{\tau}{8R_{max}}\sqrt{\frac{2\pi kT}{m}}(1 - erf(q))
\end{aligned} \tag{A8}$$

which does *not* diverge for $\omega_L \to 0$ and

$$J_{32} = \int_{R_{max}\omega_L}^{\infty} dv_\perp f_2(v_\perp) \int_{s-1}^{s+1} dx \sqrt{1 - (x-s)^2} x \left(1 - \frac{\arccos \frac{1-x^2-s^2}{2xs}}{\pi}\right) = 2q^2 \int_1^{\infty} s e^{-s^2 q^2} N_3 \quad (A9)$$

with

$$N_3 = \int_{s-1}^{s+1} dx \sqrt{1 - (x-s)^2} x \left[1 - \frac{\arccos(-1 + \frac{1-(x-s)^2}{2xs})}{\pi}\right] \quad (A10)$$

Using $z = x - s$ this becomes:

$$N_3 = \int_{-1}^{1} dz \sqrt{1 - z^2} (s+z) \left[1 - \frac{\arccos(-1 + \frac{1-z^2}{2s(z+s)})}{\pi}\right] = N_{31} + N_{32} \quad (A11)$$

with

$$N_{31} = \int_{-1}^{1} dz \sqrt{1 - z^2} z \left[1 - \frac{\arccos(-1 + \frac{1-z^2}{2s(z+s)})}{\pi}\right] \quad (A12)$$

and

$$N_{32} = s \int_{-1}^{1} dz \sqrt{1 - z^2} \left[1 - \frac{\arccos(-1 + \frac{1-z^2}{2s(z+s)})}{\pi}\right] \quad (A13)$$

If $\omega_L \to 0, s \to \infty$, and $\frac{1-z^2}{2s(z+s)} \to 0$, hence the argument of the inverse cosine is very nearly -1, and thus we have $\left[1 - \frac{\arccos(-1 + \frac{1-(x-s)^2}{2xs})}{\pi}\right] \to 0$ which gives a vanishing contribution for N_{31}. However, for N_{32} this is multiplied by $s \to \infty$ so the result is not immediately clear. Since Taylor-expanding the inverse cosine around -1 does not work due to the infinite derivative, we can use Frobenius's method or write

$$x = \frac{1-z^2}{2s(z+s)} \to 0 \quad (A14)$$

and write

$$\arccos(-1 + x) = \pi - \arccos(1 - x) \quad (A15)$$

Next, use L'Hopital's rule to evaluate as $x \to 0$

$$\frac{\arccos(1-x)}{x^{1/2}} \to 2^{1/2} \quad (A16)$$

with the final result that

$$s\left[1 - \pi^{-1}\arccos(-1 + \frac{1-z^2}{2s(z+s)})\right] \to \frac{s}{\pi}\sqrt{\frac{2(1-z^2)}{2s(z+s)}} = \pi^{-1}\sqrt{\frac{1-z^2}{1+z/s}} \to \pi^{-1}\sqrt{1-z^2} \quad (A17)$$

Therefore we again have no divergence for small q (large s); furthermore the above large s asymptotic result is useful numerically due to possible underflows of $\left[1 - \pi^{-1}\arccos(-1 + \frac{1-z^2}{2s(z+s)})\right]$.

References

1. Alexiou, S. Line Shapes in a Magnetic Field: Trajectory Modifications I: Electrons. *Atoms* **2019**, *7*, 52–63. [CrossRef]
2. Günter, S.; Köenies, A. Diagnostics of dense plasmas from the profile of hydrogen spectral lines in the presence of a magnetic field. *JQSRT* **1999**, *62*, 425–431. [CrossRef]
3. Hegerfeld, C.G.; Kesting, V. Collision-time simulation technique for pressure-broadened spectral lines with applications to Ly-α. *Phys. Rev. A* **1988**, *37*, 1488–1496. [CrossRef] [PubMed]

4.　Seidel, J.; Verhandl, D.P.G. *Spectral Line Shapes 6*; Frommhold, L., Keto, J.W., Eds.; AIP: New York, NY, USA, 1990; Volume 216.

5.　Alexiou, S. Implementation of the Frequency Separation Technique in general lineshape codes. *High Energy Density Phys.* **2013**, *9*, 375–384. [CrossRef]